Density Functional Studies on the Effects of Hydrogen Bonding on the Formation of a Charge-Transfer Complex between *p*-Benzoquinone and 2,6-Dimethoxyphenol

Prakriti Ranjan Bangal[†]

Inorganic and Physical Chemistry Division, Indian Institute of Chemical Technology, Tarnaka, Hyderabad 500007, India

Received: February 27, 2007; In Final Form: April 20, 2007

The ability to form a ground-state charge-transfer (CT) complex between an electron acceptor, *p*-benzoquinone (BQ) and an electron donor, 2,6-dimethoxyphenol (DMOPh) was found to be enhanced by H-bonding of BQ to a hydrogen-bond donor, trifluoroacetic acid (TFA) and H-bonding DMOPh to a hydrogen-bond acceptor, 4-(*N*,*N*-dimethylamino)pyridine (DMAPy) [*Chem. Phys. Lett.* **2005**, *401*, 200]. Here is reported density functional theory (DFT) calculations to study the effect of H-bonding to electron donor and electron acceptor moieties on the ground-state CT complex formation ability between the aforementioned electron donor/acceptor pair. DFT calculations using B3LYP with the 6-311G(d,p) basis set show that the HOMO and LUMO energies of BQ drop on H-bonding to TFA through its C═O groups and the HOMO and LUMO energies of DMOPh increase on H-bonding to DMAPy via its O−H group. BQ molecules hydrogen-bonded as 1:1 and 1:2 complexes to TFA act as stronger acceptors than the bare molecule, while 1:1 complexes of DMOPh and DMAPy act as better donors. Vertical excitation energies for electronic transitions from the ground state to the first few excited states of BQ, DMOPh, DMAPy, and their different complexes have been investigated in the framework of time-dependent density functional theory (TD-DFT) to simulate and interpret experimental ultraviolet absorption spectra. Good agreement between experimental and calculated spectra is established. The enhancement of the CT complex formation ability between the BQ and DMOPh pair is favored by the strong H-bonding interaction of BQ with TFA as well as by the H-bonding interaction of DMOPh with DMAPy.

Introduction

The formation of ground-state electron donor−acceptor (EDA) or charge-transfer (CT) complexes is a fundamental process, which has recently gained high importance as a possible means of producing highly efficient nonlinear optical materials.[1] In addition, CT complexes play a pivotal role in living systems, leading to natural phenomena such as proton-coupled electron transfer in the excited state, which occurs in photosystem II. Such complexes have also been reported to be important reaction intermediates.[2−7] Quinones are ubiquitous in living systems and represent important cofactors for electron transfer in photosynthesis and respiration.[8] Quinone−hydroquinone couples have been studied over many decades as the prototypical examples of an organic redox system.[9−11] Hydrogen-bonding and protonation effects in the electrochemistry of quinones in aprotic solvents have been systematically studied by Gupta and Linschitz.[12] However, in addition to their intrinsic chemical interest, these studies are particularly important in view of the key biological functions of quinone-based couples as electron−proton transfer agents in oxidative phosphorylation and photosynthesis.[13−17] Thus, it is necessary to understand, as much as possible, the environmental factors that regulate the formation of CT complexes with various electron donors that appear in quinone systems, both in vitro and in mitochondrial or photosynthetic membranes. Among these factors, we are particularly concerned here with the effect of hydrogen bonding on CT, which has been implicated in the biological function of the quinone systems[16] and on which surprisingly little research has been done. Ground-state hydrogen-bonding (HB) complexes are well-known for many systems,[18−20] but their importance on the formation of CT complexes is not yet fully explored. Indeed, references to the role of hydrogen-bonding in quinone CT complexes are remarkably sparse.[21] To address this issue, a systematic spectrometric study has been performed of CT complexes formed between BQ and aromatic donors in nonpolar aprotic solvents.[22] This work demonstrated that strongly hydrogen bonded or protonated para-benzoquinine serves as a strong electron acceptor, increasing its ground state CT complex formation ability with aromatic donors. Moreover, proton coupled charge transfer was observed in the ground state for *p*-benzoquinone (BQ) and 2,6-dimethoxyphenol (DMOPh), and on the other hand H-bonded DMOPh to 4-(*N*,*N*-dimethylamino)-pyridine (DMAPy) acted as strong donor.

In the past decade, density functional theory (DFT) calculations have been widely accepted by the quantum chemistry community as a cost-effective approach for the computation of molecular structure and the energies of chemical reactions. It is believed that the reliability of electronic structure calculations of molecular and supramolecular systems by DFT is superior to Hartree−Fock (HF) theory.[23−25] Møller−Plesset second-order perturbation theory (MP2), a post-self-consistent-field (post-SCF) method, adds electron correlation corrections to the basic HF model and provides some improvement in the accurate description of molecules at the expense of large computational cost, whereas DFT methods compute electron correlation via general *functionals* of electron density and demonstrate significantly greater accuracy than HF at only a modest increase in

[†] E-mail: prbangal@yahoo.com or prakriti@iict.res.in.

10.1021/jp071612+ CCC: $37.00
Published on Web 06/01/2007

SCHEME 1: Schematic Representation of BQ, TFA, DMOPh, DMAPy, and Their Respective Complexes

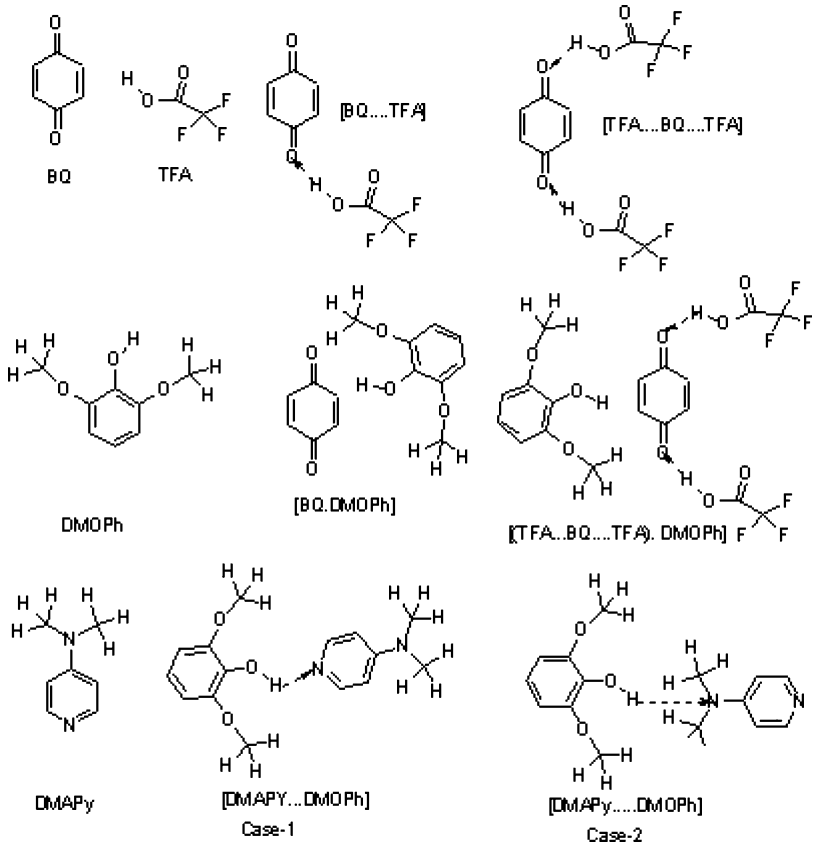

cost. In simple molecular orbital theory approaches, the HOMO energy (ϵ_{HOMO}) is related to the ionization potential (IP) by Koopmanns' theorem, and the LUMO energy (ϵ_{LUMO}) is used to estimate the electron affinity (EA). If $\epsilon_{HOMO} \approx$ IP and $\epsilon_{LUMO} \approx$ EA, then the average values of the HOMO and LUMO energies are related to the electronegativity (χ) defined by Mulliken[26] as $\chi = (IP + EA)/2$. In addition, the HOMO−LUMO gap is related to the hardness (η)[27] and also is an approximation to the first electron excitation energy. The electronegativity and hardness are used extensively to make predictions about chemical behavior.

At present, the most successful and extensively used method to calculate excitation energies and to produce electronic spectra is the time-dependent generalization of DFT theory (TD-DFT).[28−31] In addition, this method has emerged as a well-accepted standard tool for the theoretical treatment of electronic excitation spectra.[32−34] With its low computational costs, the TD-DFT method is better suited to fairly large molecular systems and their complexes than wave function based ab initio method.[35,36] Although, TD-DFT is an approximate method where adiabatic approximation (AA) is made along with[37,38] approximate (time-independent) exchange-correlation (XC) functional, AA is known to work well for low-lying excited states, well below the ionization limit.

Here I report calculations of the electronic structure and the UV−vis spectra of molecular complexes consisting of TFA as H-bond donor, DMAPy as H-bond acceptor, BQ as electron acceptor, and DMOPh as electron donor. This work is an effort to model previous experimental work from this laboratory[22] and, in particular, to search for the reason behind the enhancement of CT complex formation ability that was observed due to hydrogen bonding or protonation. This study promises to be an important tool in the quest not only to understand the mechanism of fundamental process, proton-coupled charge transfer (PCCT), but also lay the foundation for a search for novel nonlinear optical materials and organic metals.

Methods

All the molecular modeling computations were performed via the density functional methods by using the Gaussian 03, revision B.03 package[39] implemented on Intel Pentium-4 PC machines. The optimization of the geometries and population analysis were carried out using the generalized-gradient approximation Becke−Lee−Yang−Parrs BLYPd level of theory with 6-311G(d,p) basis set. The models analyzed were as follows: *p*-benzoquinone (BQ), trifluoroacetic acide (TFA), 2,6-dimethoxyphenol (DMOPh), 4-(*N*,*N*-dimethylamino)pyridine (DMAPy), [TFA···BQ], [TFA···BQ···TFA], [BQ·DMOPh], [{TFA···BQ···TFA}·DMOPh], and [DMAPy···DMOPh] (Scheme 1). Geometry optimizations were continued up to reaching the tight convergence criteria implemented in Gaussian 03. Molecular drawings were obtained through the Gauss View 03 software package.[40] [TFA···BQ] and [TFA···BQ···TFA] complexes were drawn just by placing BQ and TFA side by side in Gauss View's molecular editor. Sufficient numbers of suitable redundant coordinates were chosen in order to have optimized structures of the complexes.

A small number of low-lying singlet−singlet transitions of the closed shell monomers and complexes were calculated using TD-DFT. The ground-state geometries of the monomers and the complexes are employed throughout all calculations of their excited-state properties in the TD-DFT method. Thus, the theoretical excitation energies correspond to vertical transitions, which can be approximately identified as band maxima in experimental absorption spectra. GaussSum 0.8[41] was used to calculate group contributions to the molecular orbitals, to prepare the partial density of states (PDOS) spectra, and to convolute

TABLE 1: Calculated Total Electronic Energies of Different Individual Molecules, Formation Energies of Different Complexes, Dipole Moments, and First Three Occupied and Three Virtual Orbital Energies

compound	Energy (a.u)	ΔE (kcal/mol)	dipole (D)	occupied orbital[a] (eV)	virtual orbital[b] (eV)
BQ	−381.55		0	−7.59 H	−3.74 L
				−7.84 H-1	−1.02 L+1
				−8.52 H-2	0.06 L+2
TFA	−526.94		2.80	−8.75 H	−1.32 L
				−9.88 H-1	0.54 L+1
				−11.39 H-2	2.80 L+2
[BQ···TFA]	−908.51	−12.5	4.78	−8.13 H	−4.40 L
				−8.24 H-1	−1.55 L+1
				−8.79 H-2	−0.75 L+2
[TFA···BQ···TFA]	−1435.46	−18.80	5.30	−8.37 H	−4.93 L
				−8.41 H-1	−1.95 L+1
				−8.94 H-2	−1.12 L+2
DMOPh	−536.65		2.17	−5.49 H	0.25 L
				−6.05 H-1	0.43 L+1
				−8.32 H-2	1.12 L+2
[BQ·DMOPh]	−918.22	−12.55	1.94		
DMAPy					
	−382.35		4.62	−5.83 H	−0.18 L
				−6.68 H-1	−0.05 L+1
				−6.97 H-2	0.82 L+2
[DMAPy···DMOPh]					
case 1	−919.02	−7.9	8.95	−5.08 H	−0.57 L
				−5.66 H-1	−0.50 L+1
				−6.19 H-2	0.58 L+2
case 2	−919.013	−3.4		−5.49 H	0.10 L
				−5.92 H-1	0.19 L+1
				−6.67 H-2	0.21 L+2
[(TFA···BQ···TFA)·DMOPh]	−1972.14	−37.6			

[a] H = HOMO. [b] L = LUMO.

the calculated UV−vis spectrum. The UV−vis absorption spectra and molar extinction coefficients have been convoluted assuming a Gaussian shape of the absorption band and a full width at half-maximum (fwhm) of 4000 cm^{-1} for the monomers and 9000 cm^{-1} for CT complexes. The contribution of a group to a molecular orbital was calculated within the framework of Mulliken population analysis. The PDOS spectra were created by convoluting the molecular orbital information with Gaussian curves of unit height and of 0.3 fwhm.

Results and Discussion

Geometries and Frontier MO Calculations of the Monomers and Their Complexes. All the monomers studied were fully optimized at the B3LYP/6-311G(d,p) level. Comparative analyses with the available geometrical parameters in literature were in acceptable agreement with the optimized parameters[42] obtained. Use of the less expanded basis sets 6-31G and 6-311G did not significantly change the optimized geometrical parameters. The basis set dependence of the DFT results shows that the 6-311G(d,p) basis set is acceptable for calculating the HOMO and LUMO energies for large molecules (particularly when the HOMO and LUMO energies are negative) and their complexes for correlating the results with molecular properties. In the present study we are less concerned about the details of structural parameters and molecular properties rather our focus is on the trends in the change in the energies of the frontier molecular orbital due to H-bonded complex formation. Nonetheless, the calculated energy gap (ΔE = 3.85 eV) between HOMO and LUMO of BQ (Table 1) is in good agreement with the observed absorption band energy,[22,43] and the calculated vertical ionization potential (IP = 9.8 eV) of DMOPh. Moreover, the electron affinity (EA = 1.89 eV) of BQ, as determined from the total energy calculations on the neutral and ionic systems, gives a good match with reported values.[44,41] These comparisons highlight the reliability of this level of calculation for the studies reported here. The HOMO and LUMO energies (ϵ_{HOMO} and ϵ_{LUMO}) of DMOPh are also calculated (Table 1), and ΔE is found to be 5.24 eV. The energy difference between HOMO of DMOPh (electron donor) and LUMO of BQ (electron acceptor) is calculated to be 1.75 eV. It is apparently underestimated (red-shifted) by ∼1 eV relative to the experimentally observed CT band energy of the pair. This discrepancy between experimental and theoretical values simply does not validate ΔE to be an approximation to the first electron excitation energy of the complex. Hence, this discrepancy could be an indication of the involvement of other MO's in the formation of CT complexes (vide supra) but may also suggest the existence of vibrational coupling between the donor and acceptor. As our present goal is to determine the role of the H-bonding interactions in enhancing the formation of CT complexes and to understand the trend in this behavior, precise prediction of the position of the CT band is not necessary. Therefore, we shall not be concerned with the red shift of band position per se, but we will take it into account in comparing calculations with experiment. The dipole moment of the individual BQ, TFA, DMOPh, and DMAPy molecules are also calculated, which are 0, 2.8, 2.17, and 4.62 D, respectively. and matched well with the reported values.[45−47]

The initial structure of the 1:1 BQ−TFA complex was built by placing the OH group of TFA close to one of the C═O groups of BQ. The two molecules were constrained to be planar and coplanar with one another with the exception of the CF_3 group. The optimization was carried out at the B3LYP/6-311G-(d,p) level with the tight convergence criteria implemented in Gaussian 03. The refined O···H distance was found to be 1.74 Å, which is a bit on the shorter side of the usual hydrogen bond distance at room temperature reported elsewhere.[48] The formation energy of this [TFA···BQ] complex as computed from the total electronic energies at the B3LYP/6-311G(d,p) level, without any correction for the basis set superposition error

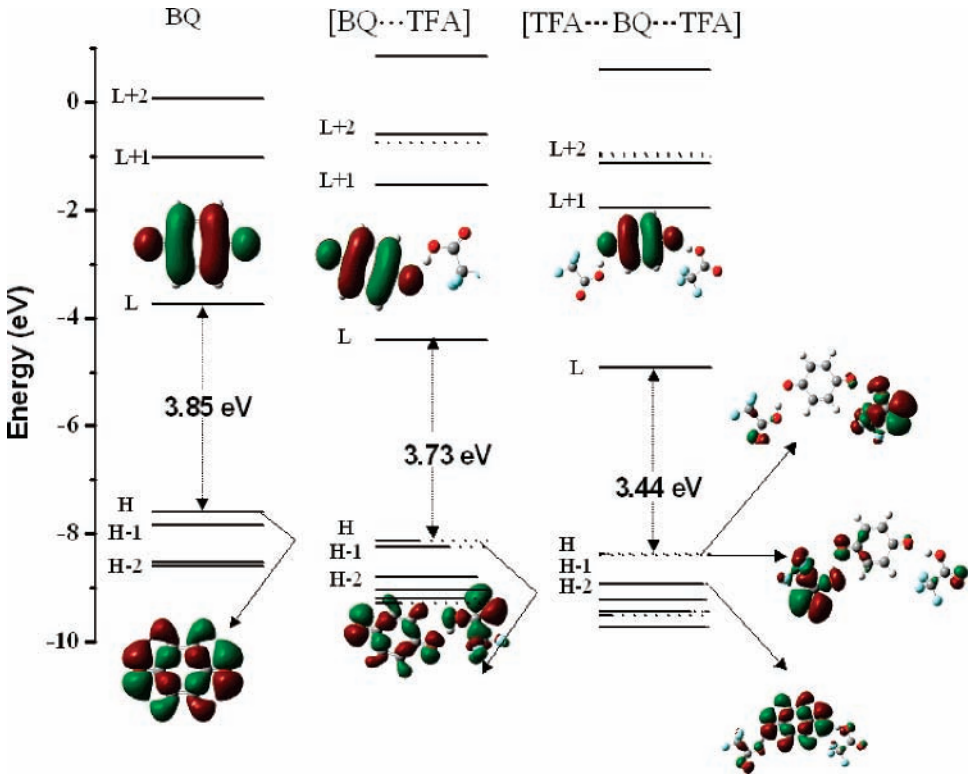

Figure 1. Calculated orbital energy levels and surface plot of frontier HOMO and LUMO of BQ and [TFA···BQ] and the surface plot of frontier HOMO, HOMO-1, HOMO-2, and LUMO of the [TFA···BQ···TFA] complex. Dotted lines represent the percentage contribution of TFA, and solid lines represent the percentage contribution of BQ on respective orbitals of the complexes.

(BSSE), is −12.5 kcal/mol, which indicates the interaction between TFA and BQ is quite strong.[48,49] This could be due to the strong acidity of TFA such that the proton can be considered to be fully transferred to the BQ moiety. It is also found that the [BQ···TFA] complex is coplanar except the CF_3 group. The dipole moment of the complex is 2-fold larger than the sum of dipole moments of individual molecules, suggesting again that the interaction between BQ and TFA is strong. This strong interaction of BQ and TFA leads to rearrangement of charge distribution over both of the molecules. The rearrangement of charge distribution upon complexation is modeled by altering the molecular orbital energy levels of BQ (Table 1). The ϵ_{HOMO} and ϵ_{LUMO} of BQ are calculated to be −7.59 and −3.74 eV, respectively. In the 1:1 complex with TFA the ϵ_{HOMO} and ϵ_{LUMO} energy levels of BQ drop to −8.13 and −4.40 eV, respectively. The percentage contribution calculation reveals that the contribution of the TFA group to the HOMO of the [BQ···TFA] is 60, whereas as no contribution is predicted for LUMO from TFA (Figure 1). The gap (ΔE) between HOMO and LUMO of BQ also decreases from 3.85 to 3.73 eV upon complex formation. Furthermore, for two sites H-bonding, i.e., the [TFA···BQ···TFA] (1:2) complex, the ϵ_{HOMO} and ϵ_{LUMO} energy further decrease (Table 1) and the HOMO−LUMO gap also decreases. In this case, HOMO and HOMO-1 are almost degenerate and more than 90% of the contribution to this orbital comes from TFA (Figure 1). Interestingly, no contribution of TFA is observed in the LUMO, and the shape of LUMO of BQ is not changed on complex formation with either one or two TFA molecules. This progressive decrease of the ϵ_{LUMO} of BQ, while keeping the shape of the spatial distribution of the orbital unaltered on forming both complexes, demonstrates that strong interaction with the TFA virtual orbitals is the energetically stabilized increasing electron affinity of the BQ. Stabilization of virtual orbital energy increases the electron affinity, which in turn, enhances the intrinsic CT complex formation ability of the H-bonded BQ. The energy difference between the HOMO of DMOPh and the LUMO of the 1:2 [TFA···BQ···TFA] complex is ∼0.56 eV, which is fairly close to the vibrational thermal energy. This result implies that the CT complex of the H-bonded BQ with DMOPh is predicted to be red-shifted by (1.75 − 0.56) 1.19 eV with respect to the CT complex of bare BQ with DMOPh if the approximation is made that ΔE is the first electron excitation energy. This result qualitatively supports our observed results where the red shift of the CT band of the [BQ·DMOPh] complex was measured as a function of TFA concentration (Figure 4S of the Supporting Information).[22] Two optimized structures of CT complexes of BQ to DMOPh and H-bonded BQ to DMOPh are shown in Figure 2. In the first CT complex of BQ to DMOPh, the two molecules are nearly coplaner and the angle between the BQ plane and the DMOPh plane is ∼170°, whereas for the second case the angle between BQ and DMOPh is ∼110°. This result also provides evidence for strong interaction between DMOPh and H-bonded BQ, which is in agreement with our previous experimental results.

On the other hand, the H-bonded DMOPh−DMAPy pair serves as a better donor than free DMOPh. We report here the effect of H-bonding interaction between these two molecules on their MOs. Two types of (1:1) H-bonding complexes were considered. In the first, the pyridine N atom forms a H-bond with the OH group of DMOPh, and, in the second, the amino N atom forms a H-bond with the OH group of DMOPh. In the first case, the initial structure was built by placing pyridine N atom of DMAPy in close proximity to the OH group of DMOPh. The two molecules were constrained to be planar and coplanar to one another. In the second case, the structure was built by placing the amino N atom of DMAPy in the proximity of OH group of DMOPh. The optimization was carried out at the B3LYP/6-311G(d,p) level using tight convergence criteria.

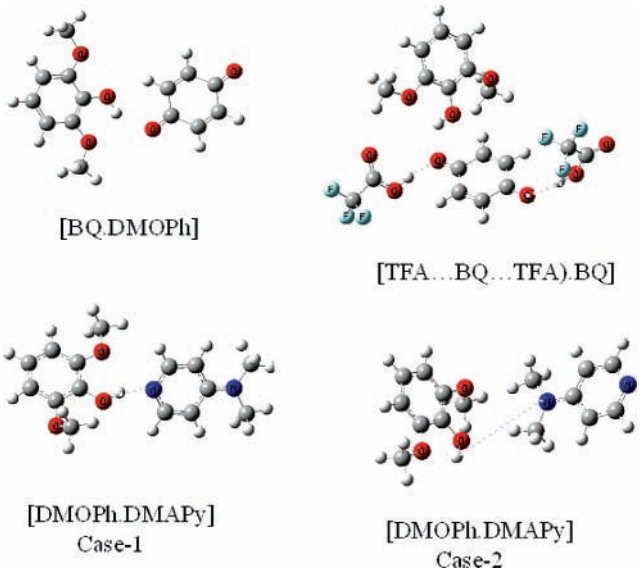

Figure 2. Optimized structure of different complexes obtained by B3LYP with the 6-311G(d,p) basis set.

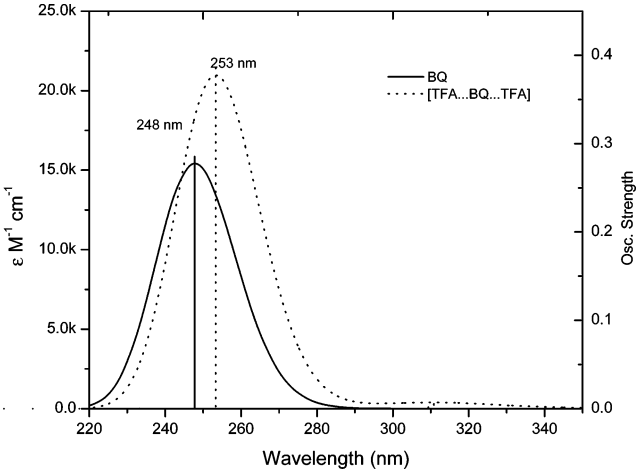

Figure 3. Convoluted calculated UV−vis absorption spectra of BQ and [TFA···BQ···TFA]. Vertical lines are the individual transitions of monomer and H-bonded complex, respectively.

Optimized structures of the complexes are shown in Figure 2. DFT calculations show that the first case is energetically more stable than the second. The interaction energy calculated for both cases are −7.9 and −3.4 kcal/mol, respectively. However, this hydrogen-bonding interaction between DMOPh and DMAPy gives rise to the HOMO and drops down to the LUMO energy levels of DMOPh, resulting in a decrease in the gap between HOMO and LUMO making it more soft and an efficient electron donor candidate. Detailed examination of the population analysis showed that there is no contribution to the HOMO orbital of the complex coming from DMAPy, although its energy increases due to the strong interaction with DMAPy. This result also supports the work of Biczok et al., where they found a decrease in the oxidation potentials of pyridine when hydrogen-bonded to phenols by voltammetric measurements.[50]

Calculation of Electronic Transitions/UV−Vis Spectra. The UV−vis spectra of BQ, DMOPh, and DMAPy show the features typical to experimental absorption spectra reported elsewhere.[51−53] TD-DFT-calculated electronic transitions were used to simulate the absorption spectra and are shown in Figure 3. Excellent agreement with the experimental spectrum of BQ was achieved, although the molar absorptivity is somewhat underestimated (15 500 M^{-1} cm^{-1} versus 22 000 M^{-1} cm^{-1}).

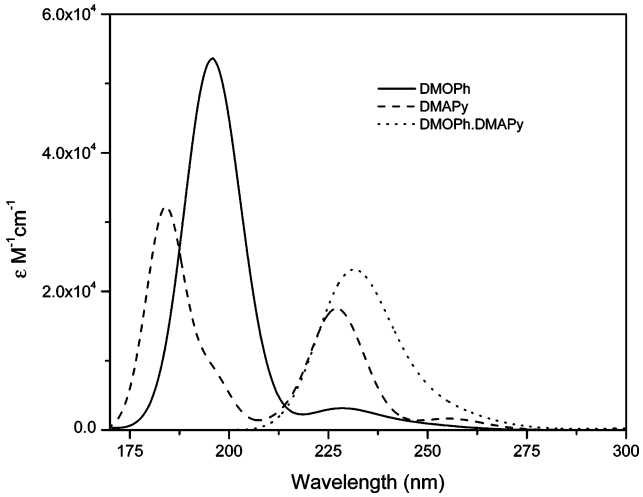

Figure 4. Convoluted calculated UV−vis absorption spectra of DMOPh, DMAPy, and [DMAPy···DMOPh].

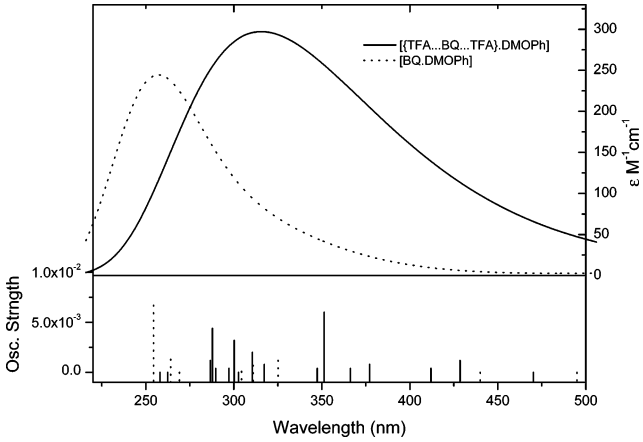

Figure 5. Convoluted calculated UV−vis absorption spectra of [BQ·DMOPh] and [{TFA···BQ···TFA}·DMOPh]. Vertical lines are the individual transitions of the respective complexes.

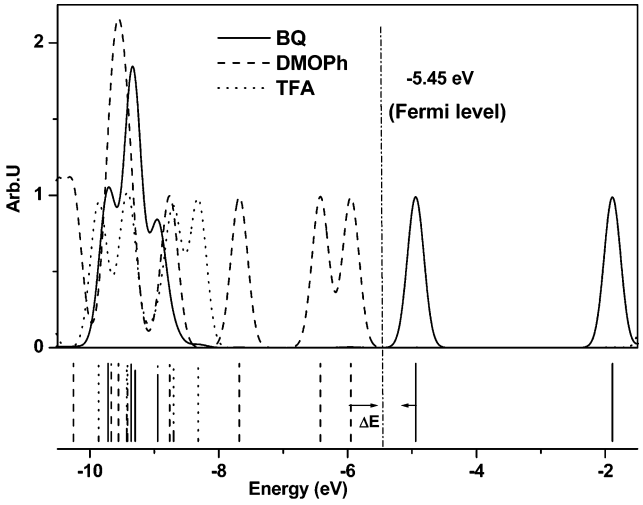

Figure 6. Partial density of state diagrams for the [{TFA···BQ···TFA}·DMOPh] complex considering BQ, DMOPh, and TFA monomers as individual groups.

A single allowed electronic transition was calculated to contribute to the $\pi\pi^*$ absorption band of BQ at 5.00 eV (245 nm, oscillator strength = 0.28). In addition, three forbidden transitions were observed in the range 2.5−3.9 eV (495−316 nm), which are $n\pi^*$ in nature. The allowed transition corresponds to nearly one-electron excitation HOMO-3 →LUMO. The calcu-

TABLE 2: TD-DFT Transition Energies and Oscillator Strengths of 10 Low-Lying Singlet Electronic Transitions of the [BQ·DMOPH] Complex with the Change of Electron Density in Associated Groups

state	energy (eV)	wavelength (nm)	oscillator strength	major contribution	change of electron density in BQ[a]	change of electron density in DMOPh[b]
S_1	1.18	1050.96	0.0005	HOMO→LUMO (100%)	1→100 (99)	99→0 (−99)
S_2	1.80	687.58	0.0002	H-1→LUMO (100%)	0→100 (100)	100→0 (−100)
S_3	2.50	494.97	0	H-2→LUMO (91%)	99→100 (1)	1→0 (−1)
S_4	2.82	440.05	0	H-3→LUMO (92%)	98→100 (2)	2→0 (−2)
S_5	3.81	325.15	0.0012	H-5→LUMO (82%)	100→100 (0)	0→0 (0)
S_6	3.99	310.92	0.0007	HOMO→L+1 (100%)	1→100 (99)	99→0 (−99)
S_7	4.07	304.35	0.0001	H-4→LUMO (99%)	0→100 (100)	100→0 (−100)
S_8	4.61	269.04	0	H-1→L+1 (100%)	0→100 (100)	100→0 (−100)
S_9	4.69	264.11	0.0013	H-7→LUMO (98%)	1→100 (99)	99→0 (−99)
S_{10}	4.87	254.33	0.0087	H-8→LUMO (91%),	4→100 (96)	96→0 (−96)

[a] BQ, group I. [b] DMOPh, group II.

lated UV−vis spectrum of [TFA···BQ···TFA] shows excellent agreement with experimentally observed spectral changes upon hydrogen bonding.[22] Figure 3 shows the increase in the absorption coefficient along with a ∼5 nm red shift of $\pi\pi^*$ absorption band of BQ that may be due to strong H-bonding of BQ to TFA. A weak band can be observed at 310 nm for the [TFA···BQ···TFA] complex, which could be the $n\pi^*$ transition and arises from nearly degenerate HOMO-5 and HOMO-6→LUMO. The main absorption band of the complex at 253 nm arises mainly from HOMO-7→LUMO, where HOMO-7 is localized on BQ along with two adjacent TFA molecules (Table 1S, Supporting Information). A nearly 5% contribution to HOMO-7 comes from TFA molecules, whereas nearly 90% of the contribution to HOMO-5 and HOMO-6 comes from TFA molecules. These observations confirm that the change of spectral behavior of BQ is due to strong interaction with two TFA molecules. UV−vis spectra calculated for DMOPh shows two moderately strong and one strongly allowed transition at 5.00 eV (248 nm, $f = 0.013$), 5.43 eV (228 nm, $f = 0.056$), and 6.28 ev (197.3 nm, $f = 0.715$), respectively (Figure 4). Similarly, UV−vis spectra simulated for DMAPy replicate the experimentally observed absorption spectra with respect to band position and molar absorption coefficient.[54] The lower energy band of DMAPy at 256 nm originating mainly from HOMO→LUMO is of $n\pi^*$ nature, and the higher energy band at 227 arises from HOMO-1→LUMO+1 and is of $\pi\pi^*$ nature. Simulated absorption spectra of [DMAPy···DMOPh] show ∼5 nm red shift of peak position relative to that of DMAPy along with an increase in molar absorption coefficient (Figure 4). This result not only confirms the hydrogen-bonding interaction between DMAPy and DMOPh is present but also provides evidence that the [DMAPy···DMOPh] complex acts as a stronger electron donor than free DMOPh.

After successful reproduction of the UV−vis spectra of the respective monomers, [TFA···BQ···TFA] and [DMAPy··· DMOPh], we examine in detail the vertical transitions of [BQ·· ·DMOPh] and the hydrogen-bonded [{TFA···BQ···TFA} · DMOPh] complexes. UV−vis spectrum of [BQ·DMOPh] shows a broad absorption band peaking at 258 nm with a low molar extinction coefficient which is composed of five weak transitions (Figure 5). The allowed transitions under the envelope of this band are vertical transitions from HOMO-5, HOMO-6, HOMO-6, HOMO-7, and HOMO-8 to LUMO and LUMO+1, and these transitions are listed in Table 2 along with the corresponding change of electron density. It is important to note that all occupied orbitals related to the transitions are localized over the BQ and DMOPh moieties with different percentage contributions, while the LUMO or LUMO+1 orbitals are completely localized on BQ. Figure 1S (Supporting Information) shows the partial density of state of the MO involved in these transitions. These results, combined with the fact that this broad band is nothing but the CT band of [BQ·DMOPh] complex. Furthermore two very weak lower energy transitions were calculated which are results of HOMO→LUMO and HOMO-1→LUMO (Table 2) and lie in the IR region. This calculated CT band is somewhat blue-shifted relative to the experimentally observed CT band.

A UV−vis spectrum simulated using TD-DFT produced 20 electronic transitions contributing to a very broad absorption band of the [{TFA···BQ···TFA}·DMOPh] complex with a maximum at 313 nm. Excellent agreement with experimental observations was achieved from the point of view of the bathochromic shift of the absorption spectrum as well as the intensity of the spectrum on going from the simple [BQ· DMOPh] complex to a hydrogen-bonded CT complex such as [{TFA···BQ···TFA}·DMOPh], though the absolute value of the peak position is bit far from the experimentally observed one. This apparent discrepancy between the experimental and calculated band positions may be explained by environmentl effects. In the DFT calculations, the complex is isolated and no solvation has been taken into account, while the experiments were carried out in methylene chloride solution, which is a polar solvent. Because the CT state is polar in nature, it is significantly stabilized in a high dielectric medium and a more red-shifted absorption band is expected than in vacuum.

The calculated spectrum of [{TFA···BQ···TFA}·DMOPh] is composed of several moderately strong transitions (Figure 5), which are associated with the promotion of electron from 14 different low-lying occupied orbitals to the first two low-lying virtual orbitals (Table 3). In the frontier region, neighboring orbitals are often closely spaced. In such cases, consideration of only the HOMO and LUMO is not realistic. For this reason, partial density of states (PDOS) diagrams, which incorporate a degree of overlap between the curves convoluted from neighboring energy levels, give a more physically meaningful picture. The PDOS diagrams for [{TFA·BQ·TFA}·DMOPh] are shown in Figure 6. Using the TD-DFT approach, the 20 lowest energy singlet transitions of the complex were calculated (Table 3). Close inspection of the relevant molecular orbitals (Figure 2S, Supporting Information) shows that all these transitions can be described as CT in nature, with a substantial contribution from TFA to enhance the formation of the CT complex. Two weak transitions resulting from HOMO→LUMO and HOMO-1→LUMO could be observed at 2426 and 1190 nm. These two transitions are CT in nature but fall outside the experimental limit of the UV−vis spectra. However, the presence of the allowed transition in the infrared (IR) region reveals that the

TABLE 3: TD-DFT Transition Energies and Oscillator Strengths of 20 Low-Lying Singlet Electronic Transitions of the [{TFA···BQ···TFA}·DMOPh] Complex along with the Corresponding Change of Electron Density in BQ, DMOPh, and TFA

state	energy (eV)	wavelength (nm)	oscillator strength	major contribution	change of lectron density in BQ	change of electron density in DMOPh	change of electron density in TFA
S_1	0.51	2426.01	0.0011	HOMO→LUMO (99%)	0→100 (100)	100→0 (−100)	0→0 (0)
S_2	1.04	1190.3	0.0001	H-1→LUMO (100%)	0→100 (100)	100→0 (−100)	0→0 (0)
S_3	2.28	544.36	0	H-2→LUMO (100%)	0→100 (100)	100→0 (−100)	0→0 (0)
S_4	2.64	470.22	0	H-6→LUMO (62%), H-4→LUMO (−11%), H-3→LUMO (19%)	55→100 (45)	4→0 (−4)	40→0 (−40)
S_5	2.89	428.52	0.0012	H-7→LUMO (15%), H-4→LUMO (11%), H-3→LUMO (62%)	23→100 (77)	2→0 (−2)	75→0 (−75)
S_6	3.01	411.95	0.0004	H-7→LUMO (54%), H-3→LUMO (−19%)	59→100 (41)	5→0 (−5)	36→0 (−36)
S_7	3.29	377.14	0.0008	H-7→LUMO (−14%), H-6→LUMO (10%), H-4→LUMO (66%)	27→100 (73)	12→0 (−12)	61→0 (−61)
S_8	3.38	366.21	0.0004	H-5→LUMO (90%)	6→100 (94)	88→0 (−88)	7→0 (−7)
S_9	3.53	351.29	0.006	H-8→LUMO (85%)	96→100 (4)	1→0 (−1)	3→0 (−3)
S_{10}	3.57	347.42	0.0004	HOMO→L+1 (100%)	1→100 (99)	99→0 (−99)	0→0 (0)
S_{11}	3.91	317.32	0.0008	H-10→LUMO (62%), H-9→LUMO (34%)	10→100 (90)	40→0 (−40)	51→0 (−51)
S_{12}	3.99	310.45	0.002	H-10→LUMO (-32%), H-9→LUMO (65%)	5→100 (95)	55→0 (−55)	39→0 (−39)
S_{13}	4.096	302.72	0	H-1→L+1 (99%)	0→100 (100)	100→0 (−100)	0→0 (0)
S_{14}	4.13	300.2	0.0032	H-11→LUMO (93%)	2→100 (98)	96→0 (−96)	1→0 (−1)
S_{15}	4.17	297.23	0.0004	H-12→LUMO (92%)	5→100 (95)	93→0 (−93)	2→0 (−2)
S_{16}	4.28	289.7	0.0004	HOMO→L+2 (98%)	0→4 (4)	100→0 (−100)	0→96 (96)
S_{17}	4.31	287.83	0.0044	H-14→LUMO (97%)	6→100 (94)	2→0 (−2)	92→0 (−92)
S_{18}	4.32	286.69	0.0012	HOMO→L+3 (97%)	1→96 (95)	99→0 (−99)	0→4 (4)
S_{19}	4.73	262.34	0	HOMO→L+4 (100%)	0→0 (0)	100→0 (−100)	0→100 (100)
S_{20}	4.80	258.07	0	H-1→L+2 (99%)	0→3 (3)	100→0 (−100)	0→96 (96)

vibronic coupling between hydrogen-bonded BQ and DMOPh might be responsible for the enhancement of allowed CT transition.

The work presented here is a model calculation where only 1:1 and 1:2 H-bonded BQ complexes were considered and is somewhat limited for this reason. There is a report pertaining to 1:4 H-bonded complexes between BQ and H_2O molecules, in which the initially quinoined structure of BQ became benzoid upon hydrogen bonding with two H_2O molecules on each side.[42] It is believed that, in the presence of a higher concentration of TFA in BQ solution, the formation of complexes containing three or more TFA molecules H-bonded to BQ is quite possible. However, this model calculation demonstrates that increasing the number of TFA molecules forming a H-bonded complex with BQ will have the trend of lowering ϵ_{LUMO} as well as the HOMO−LUMO gap. Therefore it is possible that the 1:4 or higher order H-bonded BQ complex could have a LUMO energy lower than the HOMO energy of DMOPh. This, in turn, could be the major factor giving rise to the factor of 50 times enhancement of CT complex formation ability of the H-bonded complex of BQ with DMOPh. To address this issue, detailed calculations with a large number of TFA molecules H-bonded to a BQ molecule are planned. The effect of the strength of the hydrogen-bonding interactions will also be considered by replacing TFA by other H-bonding agents.

Conclusion

The model calculations presented here qualitatively confirm that H-bonding interaction of BQ with TFA leads to the formation of stronger CT complexes between H-bonded BQ and DMOPh as compared to free BQ and DMOPh. The progressive decrease of the LUMO energy and HOMO−LUMO gap (ΔE) of BQ due to formation of 1:1 and 1:2 H-bonded complexes results in a successive increase in the electron affinity of BQ, which in turn reflects the strength of its CT complex formation ability. Similarly, complexes consisting of H-bonded DMOPh to DMAPy increases the HOMO energy of DMOPh, making it a better candidate for electron donor. TD-DFT-calculated UV−vis spectra replicate the trends in the experimentally observed absorption spectra for CT complex in terms of spectral features and band shifts toward lower energy along with the increase in the molar extinction coefficient on going from BQ/DMOPh complex to a H-bonded BQ−DMOPh complex. These frontier molecular orbital calculations not only support our previous experimental observations qualitatively but also open the new way to address fundamental issues such as proton coupled electron-transfer processes, which play an important role in PS II as well as developing new nonlinear optical materials and so-called organic metals.

Acknowledgment. Author gratefully acknowledges Professor Linda A. Peteanu for her generous help and thoughtful discussion towards the improvement of the article.

Supporting Information Available: Partial density of state diagram of [BQ·DMOPh], relevant molecular orbital surface of [BQ·DMOPH] and [{TFA···BQ···TFA}·DMOPh], and measurement of the red shift of the CT band of [BQ·DMOPh]. This material is available free of charge via the Internet at http://pubs.acs.org.

References and Notes

(1) Bella, S. D.; Fragala, I. L.; Ratner, M. A.; Marks, T. J. *J. Am. Chem. Soc*. **1993**, *115*, 682−686.

(2) Eastman, J. W.; Engelsma, G.; Calvin, M. *J. Am. Chem. Soc.* **1962**, *84*, 1339−1345.

(3) Rappoport, Z. *J. Chem. Soc*. **1963**, 4498−4512.

(4) Rappoport, Z.; Horowitz, A. *J. Chem. Soc*. **1964**, 1348−1359.

(5) Pla, F. P.; Palou, J.; Valero, R.; Hall, C. D.; Speers, P. *J. Chem. Soc., Perkin Trans. 2* **1991**, 1925−1932.

(6) Datta, K.; Mukherjee, A. K.; Banerjee, M.; Seal, B. K. *Spectrochim. Acta, Part A* **1997**, *53*, 2587−2594.

(7) Roy, T.; Datta, K.; Nayek, M. K.; Mukherjee, A. K.; Banerjee, M.; Seal, B. K. *J. Chem. Soc., Perkin Trans. 2* **1999**, 2219−2223.

(8) Trunpower, B. L. *Functions of Quinones in Energy Conserving Systems*; Academic Press: New York, 1982.

(9) Chambers, J. Q. In *The Chemistry of the Quinonoid Compounds*; Patai, S., Rappoport, Z., Eds.: Wiley; New York, 1988; Vol. II, Chapter 12, pp 719−757; Vol. I, Chapter 14, pp 737−791.

(10) Peover, M. E. *J. Chem. Soc.* **1962**, 4540−4549.

(11) Kolthoff, I. M.; Lingane, J. J. *Polarography*, 2nd ed.; Interscience: New York, 1967.

(12) Gupta, N.; Linschitz, H. *J. Am. Chem. Soc.* **1997**, *119*, 6384.
(13) Rich, P. R. *Biochem. Biophys. Acta* **1984**, *768*, 53−79.
(14) Swallow, A. J. In *Function of Quinones in Energy Conserving Systems*; Trumpower, B. L., Ed.; Academic Press: New York, 1982; Chapter 3, p 66.
(15) Trumpower, B. L. *J. Biol. Chem.* **1990**, *265*, 11409−11412.
(16) Okamura, M. Y.; Feher, G. *Annu. Rev. Biochem.* **1992**, *61*, 861.
(17) Crofts, A. R.; Wraight, C. A. *Biochem. Biophys. Acta* **1983**, *726*, 149.
(18) Lewis, F. D.; Yang, J. S. *J. Phys. Chem. B* **1997**, *101*, 1775−1781.
(19) Szafran, M. *J. Mol. Struct.* **1996**, *381*, 39−64.
(20) Del Bene, J. E.; Person, W. B.; Szczepaniak, K. *Chem. Phys. Lett.* **1995**, *247*, 89−94.
(21) Ge, Y.; Lilienthal, R.; Smith, D. K. *J. Am. Chem. Soc.* **1996**, *118*, 3976−3977.
(22) Bangal, P. R. *Chem. Phys. Lett.* **2005**, *401*, 200−204.
(23) Liu, R. F.; Dennis, R. T.; Jefferey, A. C.; Panla, R. M. *J. Phys. Chem.* **1996**, *100*, 3430−3434.
(24) Zhou, X. F.; Liu, R. F. *Spectrochim. Acta, Part A* **1997**, *53*, 259−269.
(25) Nwobi, O.; Higgins, J.; Zhou, X. F; Liu, R. F. *Chem. Phys. Lett.* **1997**, *272*, 155−161.
(26) Mulliken, R. S. *J. Chem. Phys*. **1934**, *2*, 782−793.
(27) Parr, R. G.; Pearson, R. G. *J. Am. Chem. Soc.* **1983**, *105*, 7512−7516.
(28) Jamorski, C.; Casida, M. E.; Salahub, D. R. *J. Chem. Phys*. **1996**, *104*, 5134−5147.
(29) Bauernschmitt, R.; Ahlrichs, R. *Chem. Phys. Lett*. **1996**, *256*, 454−464.
(30) Georling, A.; Heinze, H. H.; Ruzankin, S. P.; Staufer, M.; Reosch, N. *J. Chem. Phys*. **1999,** *110*, 2785.
(31) Furche, F. *J. Chem. Phys*. **2001**, *114*, 5982−5992.
(32) Parac, M.; Grimme, S. *Chem. Phys.* **2003**, *292*, 11−21.
(33) Parac, M.; Grimme, S. *J. Phys. Chem. A* **2002**, *106*, 6844−6850.
(34) Fabian, J. *Theor. Chem. Acc.* **2001**, *106*, 199.
(35) Furche, F.; Ahlrichs, R.; Sobanski, A.; Veogtle, F.; Wachsman, C.; Weber, E.; Grimme, S. *J. Am. Chem. Soc.* **2000**, *122*, 1717−1724.
(36) Ricciardi, G.; Rosa, A.; Baerends, E. J. *J. Phys. Chem. A* **2001**, *105*, 5242−5254.
(37) Gross, E. K. U.; Dobson, J. F.; Petersilka, M. In *Density Functional Theory II*; Nalewajski, R. F., Ed.; Topics in Current Chemistry, Vol. 181; Springer: Heidelberg, Germany, 1996.
(38) Casida, M. E. In *Recent Advances in Density Functional Methods*, Vol. I; Chong, d. P., Ed.; World Scientic: Singapore, 1995.
(39) *Gaussian 03*, Revision-B.03; Gaussian: Pittsburgh, PA, 2003.
(40) *GaussView3.0*; Gaussian: Pittsburgh, PA.
(41) O'Boyle, N. M.; Vos, J. G. *GaussSum 0.8*; Dublin City University: Dublin, Ireland, 2004.
(42) O'Malley, M. J. *Chem. Phys. Lett*. **1997**, *274*, 251−254.
(43) Ahmed, M.; Khan, Z. H. *Spectrochim. Acta, Part A* **2000**, *56*, 965−981.
(44) Stanton, J. F.; Sattelmeyer, K. W.; Gauss, J.; Allan, M.; Skalicky, T.; Bally, T. *J. Chem. Phys.* **2001**, *115*, 1−4.
(45) Szydlowska, I.; Kyrychenko, A.; Gorski, A.; Waluk, J.; Herbich, J. *Photochem. Photobiol. Sci.* **2003**, *2*, 187−194.
(46) Yang, T. K.; Shen, C. Y. 1,4-Benzoquinone. In *Encyclopedia of Reagents for Organic Synthesis*; Paquette, L., Ed.; Wiley: New York, 2004.
(47) Eidman, K. F.; Nichols. P. J. Trifluoroaceticacid. In *Encyclopedia of Reagent for Organic Synthesis*; Paquette, L., Ed.; Wiley: New York, 2004.
(48) Crabtree, R. H.; Siegbahn, P. E. M.; Eisenstein, O.; Rheingold, A. L.; Koetzie T. F. *Acc. Chem. Res.* **1996**, *29*, 348−354.
(49) Roy, E. B.; Roberto, L. A. H.; Antonia, T. do A. *J. Braz. Chem. Soc*. **2002**, *13*, 800.
(50) Biczok, L.; Gupta, N.; Linschitz, H. *J. Am. Chem. Soc.* **1997**, *119*, 12601−12609.
(51) Fuh, A.; Corkan, J. Li. A.; Lindsy. J. S. *Photochem. Photobiol.* **1998**, *68*, 141−142.
(52) Herbich, J.; Waluk, J. *Chem. Phys.* **1994**, *188*, 247−265.
(53) Zhang, L.; Peslherbe, G. H.; Muchall, H. M. *Photochem. Photobiol.* **2006**, *82*, 324−331.
(54) Herbich, J.; Waluk, J. *Chem. Phys.* **1994**, *188*, 247−265.